

**Variations of Cloud Condensation Nuclei (CCN) and Aerosol
Activity during Fog-Haze Episode: a Case Study from Shanghai**

Chunpeng Leng ^a, Deqin Zhang ^a, Qun Zhang ^a, Chen Xu ^a, Tiantao
Cheng ^{a,b}, Renjian Zhang ^c, Jun Tao ^d, Jianmin Chen ^{a,b}, Shuping Zha ^a,
Yunwei Zhang ^a, Xiang Li ^a, Lingdong Kong ^a, [Wei Gao^e](#)

a. Shanghai Key Laboratory of Atmospheric Particle Pollution and
Prevention (LAP³), Department of environmental science and
engineering, Fudan University, Shanghai 200433, China;

b. Fudan-Tyndall Centre, Fudan University, Shanghai 200433, China;

c. Key Laboratory of Region Climate-Environment Research for
Temperate East Asia, Institute of Atmospheric Physics, Chinese
Academy of Sciences, Beijing 100029, China;

d. South China Institute of Environmental Sciences, Ministry of
Environmental Protection, Guangzhou 510655, China;

e. [Shanghai Meteorological Bureau, Shanghai 200030, China;](#)

* Corresponding authors: Tiantao Cheng, Jianmin Chen;

Tel: (86) 21-65643230; fax: (86) 21-65642080;

Email: ttcheng@fudan.edu.cn, jmchen@fudan.edu.cn

Abstract

Measurements of Cloud condensation nuclei (CCN), condensation nuclei (CN) and aerosol chemical composition were performed simultaneously at an urban site of Shanghai from 6 to 9 November 2010. The variations of CCN number concentration (N_{CCN}) and aerosol activity (activated aerosol fraction, N_{CCN}/N_{CN}) were examined during a fog-haze co-occurring event. Anthropogenic pollutants emitted from vehicles and unfavorable meteorological conditions such as low planetary boundary layer (PBL) height exerted a great influence on $PM_{2.5}$ and black carbon (BC) loadings. N_{CCN} at 0.2% supersaturation (SS) mostly fell in the range of 994 to 6268 cm^{-3} , and the corresponding N_{CCN}/N_{CN} varied between 0.09 and 0.57. N_{CCN} and N_{CCN}/N_{CN} usually were higher in hazy case due to increased aerosol concentration in the accumulation mode (100-500 nm), and lower in foggy-hazy and clear cases. BC mass concentration posed a strong positive effect on N_{CCN} in foggy-hazy and hazy cases, whereas it poorly correlated with N_{CCN} in clear case. N_{CCN}/N_{CN} was weakly related with BC both in foggy-hazy/hazy and clear cases. By using a simplified particle hygroscopicity (κ), the calculated critical dry size (CDS) of activated aerosol did not exceed 130 nm at 0.2% SS in spite of diverse aerosol chemical compositions. The predicted N_{CCN} at 0.2% SS was very successful compared with the observed N_{CCN} in clear case ($R^2=0.96$) and foggy-hazy/hazy cases ($R^2=0.91$). In addition, their

corresponding ratios of predicted to observed N_{CCN} were on average 0.95 and 0.92, respectively. More organic matter is possibly responsible for this closure difference between foggy-hazy/hazy and clear cases. These results reveal that the particulate pollutant burden exerts a significant impact on N_{CCN} , especially N_{CCN}/N_{CN} promotes effectively during the polluted periods.

Key words: cloud condensation nuclei, fog, haze, aerosol, urban

1. Introduction

Cloud condensation nuclei (CCN), which constitutes an important fraction of atmospheric aerosol, can influence the microphysical and radiative properties and lifetime of cloud indirectly and consequently impact the hydrological cycle (IPCC, 2007). The elevated CCN loadings (N_{CCN}) tend to reduce cloud droplet size and then suppress precipitation in shallow and short-lived clouds (Lohmann and Feichter, 2005). But it can promote great convective overturning and enhance precipitation in deep convective clouds (Rosenfeld et al., 2008). Numerous aerosol properties, including particle size distribution, chemical composition and mixing state, are closely linked with the ability of particles to take up water vapor, i.e. the ability to act as CCN (Baumgardner et al., 2003; Kuwata and Kondo, 2008; Cubison et al., 2008). To date, the current assessment of aerosol indirect effects induced by increasing

anthropogenic aerosols remains poorly understood, and this brings a big uncertainty in fully picturing climate change (Andreae et al., 2005; IPCC, 2007).

Owing to advanced instrument development, the aerosol-cloud interaction and its impact on climate have attracted increasing attention in the last decades. Many ground-based measurements on CCN have been performed in diverse environments, describing a global map of CCN distribution in the surface atmosphere (Baumgardner et al., 2003; Yum et al., 2004, 2005; Reade et al., 2006; Juranyi et al., 2010; Leng et al., 2013). In urban environments, the new particle formation and growth, and haze pollution were observed recently as having a significant impact on N_{CCN} (Ritesh et al., 2007; Kuang et al., 2009). In recent years, CCN studies have raised the relative importance of several influence factors controlling aerosol CCN activity, of which size has been announced as the major factor in determining the CCN activation of aerosol particles (Dusek et al., 2006; Anttila and Kerminen, 2007; Hudson, 2007; Quinn et al., 2008; Jimenez et al., 2009; Leng et al., 2013). However, how chemical composition especially organic compounds to link with aerosol activity and then CCN has not been fully understood. In fact, up to 90% of the aerosol population has been formed by carbonaceous substances, and among them 10-70% is water-soluble (Moffet et al., 2008; Stone et al., 2008). Particularly, various externally or internally-mixed particulate

89 components comprised in urban air mass can significantly affect the
90 CCN-sized spectra of atmospheric particles (Svenningsson et al., 2006;
91 Reade et al., 2006; Kuwata et al., 2007). This has posed a major challenge
92 to study aerosol composition and predict CCN activity (Hagler et al.,
93 2007; Hings et al., 2008; Henning et al., 2010).

94 Due to rapid industrialization in Asia for decades, anthropogenic
95 particles and relevant precursor emissions have increased significantly,
96 and numerous studies have indicated that the increasing anthropogenic
97 aerosol loading has significantly changed cloud microphysical and
98 radiative properties (Streets et al., 2000, 2008; Shao et al., 2006; Wang et
99 al., 2006; Qian et al., 2006; Rosenfeld et al., 2007; Matsui et al., 2010;
100 Zhang et al., 2013). In China, studies on CCN have been done widely
101 such as at polluted sites located in Yufa (Wiedensohler et al., 2009),
102 Beijing (Yue et al., 2011), Shouxian (Liu et al., 2011) and Shanghai (Leng
103 et al., 2013), and suburban sites in Guangzhou (Rose et al., 2010, 2011)
104 and Wuqing (Deng et al., 2011). To our knowledge, little attention has
105 been paid on the impacts of fog or haze on CCN and activated aerosol
106 particles. The increases of haze occurrences are evident in the eastern and
107 southwestern cities in China (Che et al., 2009). Shanghai is a huge
108 metropolis in China, and the occurrence intensity of foggy and hazy days
109 on annual time scale has been increasing gradually especially in winter
110 (Tie and Cao, 2009), which is deeply affected by fine particle pollution

enhancement and possibly linked with particle hygroscopicity (Ye et al., 2011).

This study presents continuous measurements of CCN and aerosol during a fog-haze episode from 6 to 9 November 2010 in Shanghai. The aim is to provide insights on CCN and aerosol activity variations under fog-haze co-occurring conditions. The instrumentation and data used in the study are described in section 2. The aerosol physical and chemical properties are introduced in section 3. Section 4 presents the evolution of CCN and aerosol activity. The relationship between aerosol and CCN is discussed in section 5. Conclusions from the study are given in section 6.

2. Methods

2.1 Observational Site

The instruments for CCN and aerosol measurements have been mounted roughly 20 m above ground on the roof of a building in the campus of Fudan University in Shanghai (31°18'N, 121°29'E) since October 2010. The site is surrounded by populated residential and commercial areas, as well as urban streets. The East China Sea is roughly 40 km east of the site, and the prevailing wind directions are southeasterly in summer and northeasterly in winter. Local time (LT) hereafter employed in this study is 8h ahead of UTC.

2.2 Measurements and Methodology

N_{CCN} was measured using a continuous flow and single column CCN

counter (model CCN-100, Droplet Measurement Technologies, USA), in which an optical particle counter (OPC, 0.75-10 μ m) is employed to detect activated cloud droplets (Roberts and Nenes, 2005; Lance et al., 2006). The instrument was housed in an air-conditioned weather-proof container with temperature maintaining at 20°C. The ambient aerosol airflow passed through a dryer (active carbon) to lower relative humidity below 30% before entering the instrument (Leng et al., 2013). The CCN counter was calibrated using ammonium sulfate before the study, as did calibrations for temperature gradient, flow, pressure and OPC to maintain stable SS according to the DMT operation manual. In order to ensure accurately counting, zero checks were performed before and after the campaign and regularly every two months. The effective water vapor supersaturation (SS) changed alternately at 0.2% interval within 0.2-1.0%. In real atmosphere, SS varies from slightly less than 0.1% in polluted conditions to over 1.0% in clean-air stratus cloud (Hudson and Noble, 2014). The selection of SS 0.2% in the present study would benefit to the measurements in the urban environment for further analysis. Although the CCN counter can operate well under conditions of particles only in a few thousand number per cubic centimeter and corrections must need for larger concentrations ($>5000\text{cm}^{-3}$) (Latham and Nenes., 2011), we still used the measured N_{CCN} directly at 0.2% SS in this study since it seldom reached the upper limit.

A high-resolution wide-range particle spectrometer (WPS-1000 XP, MSP) was employed to observe particle size distributions in the size range of 10 nm-10 μm . The principles of the instrument, which have been introduced in detail by Gao et al (2009), combines the Laser Light Scattering (LPS), Condensation Particle Counting (CPC) and Differential Mobility Analysis (DMA). The DMA and CPC can effectively measure aerosol particles distributed in the size range of 10-500 nm in up to 96 channels. In 24 additional channels, the LPS spans the size range of 350-10,000 nm. In the present study 60 channels in DMA and 24 channels in LPS for the sample mode were chosen and 3 minutes were needed to scan the entire size range completely, as it took 2 seconds for scanning each channel. DMA was calibrated with NIST SRM 1691 and SRM 1963 PSL spheres (mean diameter of 0.269 and 0.1007 μm , respectively) to maintain DMA transfer function properly and accurate particle sizing traceable to NIST. Four NIST traceable sizes of PSL (i.e. 0.701, 1.36, 1.6 and 4.0 μm) were used to calculate LPS. The calibration and operating methodology of WPS has been described elsewhere (Zhang et al., 2010). In addition, we have compared the aerosol size spectra measured by WPS with those measured in parallel by a calibrated scanning mobility particle sizer (SMPS, TSI 3080) with higher accuracy in the size range of 20-800 nm, including size-resolved particle concentrations and peak sizes, and a strong correlation between them was

derived with correlation coefficient $R^2 > 0.95$ (Leng et al., 2013). The result confirms the reliability of WPS measurements for successfully characterizing the number concentration and size distribution of condensation nuclei (CN).

Planetary boundary layer (PBL) height and aerosol vertical extinction profile were measured using a set of micro pulse lidar (MPL) system (MPL-4B-532) with pulse energy 6-10 μJ and pulse repetition frequency 2500 Hz. The MPL is an eye safe, compact and autonomous instrument, and an effective tool used widely in the world to provide available high spatial (30 m) and temporal resolution (30 s) information of aerosol vertical distributions (Menut et al. 1999; Cohn and Angevine, 2000; Brooks, 2003). The range of lidar is roughly 30 km at night and 10 km during the daytime. The description of the retrieval of aerosol parameters by the MPL will be only briefly summarized here as it has been given by He et al (2006). The vertical profile of the aerosol extinction coefficient is determined by a near end approach in solving the lidar equation (Fernald, 1984). The PBL height is determined by the MPL lidar at the altitude where a sudden decrease of scattering coefficient occurs (Boers and Eloranta, 1986). The overlap problem must be solved because it can lead to an underestimation of aerosol backscatter and extinction coefficients in the lowest altitudes having the majority of aerosols (He et al., 2006a). Outlined by Campbell et al (2002), overlap is

typically solved experimentally. The system is set to point horizontally to an averaged data sample with no obscuration, such as the late afternoon, when the atmosphere is well mixed and the aerosol loading is low. The backscattering over the target layer is roughly assumed constant. The similar calibration has been performed before this study.

An online Aethalometer (AE-31, Magee Scientific Co., Berkeley, California, USA) was employed to measure black carbon (BC) at a 5-min time resolution. The instrument was operated at an airflow rate of 5 l/min. Based on the strong absorptivity of BC to light at near infrared wavelengths (Hansen et al., 1984; Weingartner et al., 2003), BC concentration is determined using the measured light attenuation at 880 nm and the appropriate value of specific attenuation cross section proportional to BC mass (Petzold et al., 1997). The attenuation can be obtained by calculating the difference between light transmission through the particle-laden sample spot and the particle-free reference spot in the filter (Cheng et al., 2006; Dumka et al., 2010). The operation, calibration and maintenance of AE-31 have been described in detail by Cheng et al. (2010).

An online analyzer for Monitoring Aerosols and Gases (MARGA, ADI 2080, Netherlands) was employed to measure the concentration of major inorganic water-soluble ions (e.g. Na^+ , K^+ , Mg^+ , Ca^+ , SO_4^{2-} , Cl^- , NO_3^- and NH_4^+) in ambient aerosol particles at 1-hour time resolution. An

air pump controlled by a Mass Flow Controller (MFC) draws ambient air with airflow of 1 m³/hour into the Sample Box. An internal calibration method by using bromide for the anion chromatograph and lithium for the cation chromatograph was operated over the entire measurement period to ensure this instrument to identify and measure ion species successfully.

Instructions for the methods of sampling, operation and internal calibration have been described in detail elsewhere (Du et al., 2011).

Moreover, the mass concentrations of particulate matter (PM) with aerodynamic diameter less than 2.5 µm (PM_{2.5}), meteorological factors and atmospheric visibility were measured by a continuous PM ambient monitor (FH62C14, Thermo), an automatic weather monitoring system (HydroMetTM, Vaisala) and a automatic visibility monitor at 5-min time resolution, respectively.

2.3 Air Mass Backward Trajectory

The HYSPLIT-4 model developed by the Air Resources Laboratory (ARL) of the National Oceanic and Atmospheric Administration (NOAA), USA (Draxler et al., 2003), was employed to compute 24h air mass backward trajectories ending at 500m height (AGL) and starting at 0:00 LT and 12:00 LT for each day. By doing so, we can identify aerosols from different source regions and analyze their effects on aerosol activity to compile a full view of the relation between fog-haze event and N_{CCN}. According to these calculated trajectories plotted in Figure 1, aerosol was

classified into two categories: (1) maritime aerosol transported by air masses from marine areas on 6 Nov. 2010 carrying dominant oceanic particles, (2) continental aerosol in air mass traveling a long distance over inland areas on 7, 8 and 9 Nov. 2010 and carrying more anthropogenic particles (e.g. BC). Exactly, the maritime air mass originated from the China Eastern Sea, traveled northwesterly slow-moving across the Hangzhou Bay and finally arrived in Shanghai on 6 November. Then the air mass changed its direction to southeasterly at around 12:00 am on 7 November, and originated from northern inland areas and traveled across the North China Plain (NCP) and the eastern region of China. The continental sources contained increasing industrial and agricultural emissions (e.g. biomass burning) due to long-term rapid economy growth and large population in the last few decades. We hope to better understand the impact of aerosols with or without anthropogenic particulate pollutants on CCN in this study by comparing these two categories.

3. Results

3.1 Overview of the Fog-haze Event

Haze is traditionally defined as an atmospheric phenomenon that the sky clarity is obscured by dust, smoke and other dry particles, and atmospheric visibility and relative humidity (RH) are usually less than 10 km and 80% over one haze episode (Fu et al., 2008). The high frequency

265 of haze or hazy days is observed in winter, especially in the urban
266 environments of northern China (Sun et al., 2006). During the haze event,
267 the enhancement of particulate pollutants may greatly affect aerosol
268 activity and N_{CCN} . The study performed in the Indo-Gangetic plain shows
269 that winter haze exerts a significant impact on the fog and low-cloud
270 formation (Gautam et al., 2007). Fog can be viewed as a
271 lower-atmospheric near-surface cloud, and plays an important role in
272 processing aerosol particles and trace gases (Gultepe et al., 2007; Biswas
273 et al., 2008). On one hand, physically similar to cloud droplet, fog droplet
274 also forms by water vapor condensing on dry aerosol particle under
275 supersaturated conditions. On the other hand, generally formed in the
276 shallow boundary layer containing local emissions, urban fog traps more
277 pollutants than cloud at high altitudes (Fisak et al., 2002; Herckes et al.,
278 2007). The fog or foggy case is defined as a weather with patterns of low
279 visibility (<10 km) and higher RH (>90%). When 80% <RH< 90%, the
280 weather was referred as a complex of haze and fog co-occurring (e.g.
281 foggy-hazy) in the present study. Figure 2 and 3 show a 4-day time series
282 of pressure, atmospheric visibility, RH, temperature, wind speed and
283 direction, and PBL height from 6 to 9 November 2010. In fact, since RH
284 seldom reached up to 90%, thus the period focused in the present study
285 were characterized as hazy and foggy-hazy cases. The haze pollution
286 lasting at least 4 hours has been identified as one haze event by an earlier

study in Shanghai, where authors paid attention to the formation of haze pollution (Du et al., 2011).

As shown in Figure 2-8, the 4-day period was classified into three parts: a hazy episode (marked in black open boxes) from 22:00 to 23:00 LT on 6 Nov. and 10:00 LT on 7 Nov. to 13:00 LT on 8 Nov., a foggy-hazy episode (marked in red open boxes) from 23:00 LT on 6 Nov. to 10:00 LT on 7 Nov., and the rest for clear episode. Statistics for meteorological conditions is listed in Table 1. During the hazy and foggy-hazy case, the average atmospheric visibility was about 4.44 km and 2.33 km, respectively, much lower than 15.4 km in the clear case. The winds from the east and the south brought clean maritime aerosol during the clear case, however, the winds from the north and the west brought polluted anthropogenic aerosol during the hazy and foggy-hazy cases. The particulate and gaseous matters, including pollutants (e.g. BC) emitted from agricultural biomass burning were transported along the air mass pathways (Figure 1), led to a significant enhancement of aerosol extinction coefficient (Figure 3). In addition, the PBL height downed to below 500 m and further suppressed the dilution of pollutants.

3.2 Physical and Chemical Properties of Aerosol

In order to visually identify aerosol evolution, particles in the size range of 10 nm to 10 μ m were categorized into 7 sub-size bins: 10-20 nm (nucleation mode), 20-50nm and 50-100nm (Aitken mode), 100-200nm,

200-500nm and 0.5-1 μm (accumulation mode), and 1-10 μm (coarse mode) (Figure 4). The similar classification has been done in the measurements at the same site by Zhang et al (2010). In this study, the integrated particle size-resolved number concentrations (N_{CN}) exhibited a regular diurnal cycle, with two peaks (9,000-16,000 cm^{-3}) almost within the traffic rush hours. The mean N_{CN} exhibited no obvious difference between the foggy-hazy (8,367 cm^{-3}) and clear (8,956 cm^{-3}) cases, but it showed a higher value (10,500 cm^{-3}) in the hazy cases, revealing a larger loading of particulate pollutants.

In general, the 20-100 nm (Aitken mode) particles are mostly dominant in all size particles probably due to local traffic emissions and meteorological conditions (Ferin et al., 1990). The temporal variation trend of Aitken mode was similar to N_{CN} . It was interesting that the particles of 100-500 nm (accumulation mode) dominated in N_{CN} in the hazy case with peak concentrations higher than 7,500 cm^{-3} , almost twice as much as the clear case (4,000 cm^{-3}). However, the foggy-hazy case is comparable to the clear case, showing a mostly unchanged evolution of the fractions of individual size bin to total particles and N_{CN} . Figure 5 shows the average size distributions for all the three cases. It is very visible that it contains relatively more large-sized (e.g. 100 nm) aerosol particles in the air during the hazy case than that during the clear and foggy-hazy case. Especially aerosol particles larger than 200 nm (typical

CCN size at SS 0.2%) were significantly enhanced.

Figure 6 shows the temporal variations of eight major inorganic water soluble ions in aerosol particles and four gaseous pollutants sampled during this study period. Measurements for SO_4^{2-} , Cl^- and NO_3^- were unavailable from 10:00 LT on 7 Nov. to 8:00 LT on 8 Nov. Substantially, the average concentration of aerosol total water soluble ions (TWSI) in the hazy case ($54.52 \mu\text{g m}^{-3}$) was comparable to the foggy-hazy case ($50.37 \mu\text{g m}^{-3}$), and roughly 2 times that of the clear case ($26.22 \mu\text{g m}^{-3}$). For the percentage of individual ions in TWSI, NH_4^+ and K^+ were relatively higher by a factor of 1.8 in the hazy and foggy-hazy cases than in the clear case. Despite the lack of SO_4^{2-} and NO_3^- partly during the hazy case, we can still conjecture their promotion on the basis of their gaseous precursor evolution of SO_2 and NO_2 .

Gaseous pollutants are released into the atmosphere from natural and anthropogenic emissions. Among them, SO_2 is known as one of the most important gaseous pollutants and a precursor responsible for acid rain. Also, it can participate in the formation of new particles through converting into gaseous H_2SO_4 , which is the most common nucleation species due to its low vapor pressure at typical atmospheric temperature (Zhang et al., 2006b; Urone et al., 1968). Secondary aerosols produced from the formation of new particles contribute more to the global aerosol burden than primary aerosols and are important sources of CCN

(Merikanto et al., 2009; Yu et al., 2008). Recent studies have shown the enhanced solubility of SO₂ due to its reaction in fog droplets during a severe fog measured in the North China Plain, and this finding has provided important support for better understanding of the acidity in clouds (Zhang et al., 2013). NO₂ mainly comes from vehicle traffic emissions in urban areas (Wang et al., 2006). Nitrogen oxides (NO, NO₂, N₂O₅) undergo heterogeneous reactions with aerosol particles (e.g. sea salt or dust) during they are transported in the atmosphere (Elizabeth et al., 2006). Thus, high gaseous pollutant content can result in larger CN loadings and subsequently more CCN particles in the atmosphere. On the whole, the loading of these precursor gases in the foggy-hazy and hazy cases exceeded that in the clear case, specifically NO₂ by a factor of 2 and SO₂ by a factor of 1.5. Moreover, SO₂ and NO₂ concentrations reached their peaks around 0:00 LT on 8 November corresponding to the highest levels of CCN and aerosol activity, implying their potential effects on CCN production, which will be discussed in the next section.

3.3. CCN Concentration and Aerosol Activity

3.3.1 CCN and Aerosol Activity

Figure 7 presents the temporal variations of N_{CCN} and activated aerosol fraction (N_{CCN}/N_{CN}) at SS 0.2%, N_{CN}, and BC during the campaign. Totally, N_{CN} fell in the range of 4,270-15,771 cm⁻³ and averaged at 9,344 cm⁻³, and N_{CCN} varied between 994 cm⁻³ and 6,268 cm⁻³

and averaged at $2,929 \text{ cm}^{-3}$. High $N_{\text{CCN}}/N_{\text{CN}}$ (0.41) and N_{CCN} ($4,362 \text{ cm}^{-3}$) were observed during the hazy case, followed by the foggy-hazy (0.29, $2,377 \text{ cm}^{-3}$) and clear (0.28, $2,432 \text{ cm}^{-3}$) cases (Table 2). The temporal variation of $N_{\text{CCN}}/N_{\text{CN}}$ and N_{CCN} was closely related with aerosol particle size spectra and chemical composition such as accumulation mode (100-500 nm) and water soluble ion content (Figure 4 and 6). Figure 8 gives the temporal variations of number concentrations of larger aerosol particles (e.g. particles larger than 80 nm and 100 nm) and their corresponding ratios with N_{CCN} at SS 0.2%. The larger aerosol particles showed significant increase during the hazy case and varied strongly correlated with N_{CCN} . More fractions of particles larger than 80 nm were activated into CCN during the hazy case (86%) and foggy-hazy case (84%) than that during the clear case (76%).

Although in different SS conditions, N_{CCN} was measured at other urban or urban-like environments such as the west coast of Tasmania (32 cm^{-3}) and the west coast of Korea ($5,292 \text{ cm}^{-3}$) at SS 1.0% (Yum et al., 2004, 2005), and Mexico city ($3,000 \text{ cm}^{-3}$), Ireland (208-346 cm^{-3}) and Vienna (820 cm^{-3}) at SS 0.5% (Baumgardner et al., 2003; Reade et al., 2006; Burkart et al., 2011). An even larger N_{CCN} ($6,000 \text{ cm}^{-3}$) was measured at SS 0.17% in Beijing (Deng et al., 2011). The average $N_{\text{CCN}}/N_{\text{CN}}$ of this study (0.32) was higher than that measured in Vienna (0.13 at SS 0.5%, CN 13-929 nm) and Finland (0.1-0.3 at SS 0.2%, CN 3-1000 nm). The

increased N_{CCN}/N_{CN} was derived at larger SS in urban environments such as Shanghai (0.47 at SS 0.8%, CN 10-10,000 nm) and Korea (0.64 at SS 1.0%, CN 10-500 nm) (Yum et al., 2005; Burkart et al., 2011; Sihto et al., 2011; Leng et al., 2013).

As expected, N_{CN} behaved in diurnal cycle with an apparent pattern of bi-modal distribution, and N_{CCN} showed a similar temporal variation (Figure 7). N_{CN} and BC usually peaked, and reached their highest values of $15,000\text{ cm}^{-3}$ and $35\text{ }\mu\text{g m}^{-3}$ during the rush hours (i.e. 7:00-9:00 and 16:00-19:00 LT), indicating that the anthropogenic pollutants emitted from vehicles contributes to a large part of CN and BC loadings. In addition, the favorable meteorological conditions such as low wind speed, temperature and planetary boundary layer (PBL) height also posed a great influence on $PM_{2.5}$ and BC loadings (Figure 3). For example, $PM_{2.5}$ and BC accumulated in mass concentration and reached their maximums when these meteorological parameters remained at low level (e.g. wind speed at 2 m s^{-1} , PBL height around 0.5 km. The later disappearance of the pollutants at the end of the hazy case was mostly attributed to the wind speed increasing from 2 to 6 m s^{-1} , and the PBL height rising from 0.4 to 1.4 km (Figure 2).

In a broad view, N_{CCN} showed a sharp increase starting at 0:00 LT on 8 Nov., and rose from 994 cm^{-3} to 6268 cm^{-3} within less than 10 hours. Similar to N_{CCN} , BC also rose from $10\text{ }\mu\text{g m}^{-3}$ to $35\text{ }\mu\text{g m}^{-3}$ during the

same period. N_{CN} was consistent with N_{CCN} , and they varied almost synchronously. However, $N_{\text{CCN}}/N_{\text{CN}}$ changed in one step mostly opposite to N_{CCN} and N_{CN} (Figure 7). The possible reason for this contradictory tendency of N_{CN} enhancement vs. $N_{\text{CCN}}/N_{\text{CN}}$ reduction is that the unactivated nanoparticles, which burst partly from primary emissions of vehicles and/or partly from secondary particles due to the chemical reactions of atmospheric gaseous precursors (Figure 5) (Du et al., 2011), contributes relatively larger to N_{CN} other than N_{CCN} .

3.3.2 Black Carbon and CCN

As a part of hydrophobic aerosols, pure BC particles acquire hydrophilic coatings as they age in the atmosphere, and then the aged BC becomes sufficiently hydrophilic and serves as CCN for cloud condensation formation (Ritesh et al., 2007). On the other hand, BC particles can release sensible heat by effectively absorbing solar radiation, thereby increasing the critical supersaturation of CCN and preventing aerosol to act as CCN (Conant et al., 2002). Biomass burning emits a large amount of trace gases and carboneous particles into the atmosphere, and leads to changes in climate and precipitation, as well as aquatic and terrestrial ecosystem (Andreae et al., 2004). The wild fires contribute a significant fraction of global CCN burden (Pierce et al., 2007; Andreae et al., 2009). Large quantities of active agricultural fire sites were detected from satellites over China on 7 November 2010 (Figure 1), whereas no

obvious wild biomass burning activities were observed during the rest days. Based on the calculated 24-h air mass backward trajectories, the air mass that passed right through the agricultural fire regions in the Jiangsu and Anhui provinces on 7 November reached the sampling site in the next day, bringing large quantities of aged BC particles after a long range transport. This resulted in a severe increase of particle mass concentration and a significant **enhancement** of aerosol extinction coefficient on 7 and 8 November (Figure 3). As discussed in section 3.2, NO_2 and SO_2 concentrations increased synchronously during the whole period (Figure 6), and they would undergo heterogeneous reactions on the surface of BC particles to change particle microphysical and chemical properties, making BC particles sufficiently hydrophilic to act as CCN (Ritesh et al., 2007).

Relationship analyses between N_{CCN} , $N_{\text{CCN}}/N_{\text{CN}}$ and BC were calculated using hourly-averaged data, and the correlation coefficients (R^2) are **presented** in Figure 9. Surprisingly, BC strongly correlated with N_{CCN} ($R^2=0.85$) in the foggy-hazy and hazy **cases**, whereas they showed a poor linear relationship ($R^2=0.25$) in the clear **case**. The possible reason is BC particle aging by heterogeneous reactions with gaseous pollutants (e.g. NO_2 and SO_2) to be activated CCN during pollutant atmospheric transport (Ritesh et al., 2007). In addition, so many studies have proposed that the aged BC is efficient CCN (Dusek. et al., 2006; Anttila and Kerminen,

2007; Hudson, 2007). However, N_{CCN}/N_{CN} was poorly related with BC for both foggy-hazy/hazy and clear cases ($R^2=0.43$ and 0.07 , respectively), indicating that BC maybe a relatively more important contributor to unactivated particles especially in nanoscale sizes (e.g. traffic emission) than activated CCN.

3.4. Relationship of Aerosol and CCN

Although aerosol size distributions were measured only in the size range of 10-10,000 nm, they were still used to predict N_{CCN} according to Köhler theory (Köhler et al., 1936). Toward this end, the particle hygroscopicity “kappa” (κ) was used in the closure calculation. The description of the technique has been given by Petters and Kreidenweis (2007), therefore it will only be briefly summarized here. The κ parameter for one multicomponent particle can be obtained through weighting each component κ_i by their volume fractions in the mixture,

$$\kappa = \sum_i \varepsilon_i \kappa_i \quad (1)$$

where ε_i is the volume fraction of chemical compounds in particles, and κ_i is the effective κ of individual chemical composition.

Assuming aerosol particles are completely internal-mixed, a simplified κ was calculated using water soluble inorganic ions (organic matter data is unavailable). Aerosol particle compositions were classified into three categories (Petters and Kreidenweis, 2007; Wiedensohler et al., 2009), and κ_i and densities for each component are shown in Table 3, in which

‘others’ is defined as ‘PM_{2.5}-BC-inorganic ions’. The critical dry size (CDS) of particle to be activated as CCN at one SS can hence be determined by the following equation:

$$S(D) = \frac{D^3 - D_d^3}{D^3 - D_d^3(1 - \kappa)} \exp\left(\frac{4\sigma_{s/a}M_w}{RT\rho_w D}\right) \quad (2)$$

where ρ_w is the density of water, M_w is the molecular weight of water, $\sigma_{s/a}$ is the surface tension of the solution/air interface, R is the universal gas constant, κ is the hygroscopicity parameter, T is temperature, D_d is the dry diameter, D is the diameter of the droplet and $S(D)$ is the critical dry size under a given SS. Detailed information for the derivation of equation (2) can be found in Petters and Kreidenweis (2007). Equation (2) applies over the entire range of humidity and solution hygroscopicity and can be utilized to predict the conditions of cloud droplet activation. The critical SS for a selected dry size of particle is determined from the maximum of the curve for equation (2). Computed for $\sigma_{s/a}=0.072 \text{ J m}^{-2}$ and $T=298.15 \text{ K}$, the calculated CDS varied between 60 nm and 130 nm and averaged at 102 nm. Particularly, the hourly-averaged CDS during the foggy-hazy/hazy cases was slightly lower (96 nm) than during the clear case (105 nm). So far, the comparable or relatively higher CDS has also been found in diverse regions and for various aerosol types, despite of different calculation models and SS. For example, the fresh aerosol particles emitted by an aircraft internal combustion engine have a CDS range of 146-301 nm at SS 0.7%, depending on varying operating

conditions (Hitzenberger et al., 2003). Furutani et al (2008) investigated three types of aerosol masses along the southern coast of California, and the CDS was estimated at 110 nm at SS 0.6% for fresh ship exhaust, 70-110 nm for fresh anthropogenic aerosols and roughly 50 nm for aged anthropogenic and clean maritime aerosols. In Vienna, the CDS has a wide gap between 69 nm and 368 nm, and averaged at 169 nm (Burkart et al., 2011). Quinn et al (2008) observed the CDS in a narrow range of 70-90 nm for maritime aerosols in the Gulf of Mexico, and a moderate range of 90-170 nm in the ship channels of Houston with high marine traffic densities close to industrial and anthropogenic sources.

The CCN population can be effectively viewed as a subset of measured aerosol size distributions since the operating range (10-10,000 nm) includes the majority of atmospheric particles. Therefore, the predicted N_{CCN} can be calculated through integrating particles upward in size from the bottom CDS to the upper boundary. In this calculation, the predicted N_{CCN} of hourly-averaged were compared with the measured ones correspondingly.

The results of this closure analysis are shown in scatterplot in Figure 10 and 11. The prediction for CCN is generally success throughout the entire data set. The linear regression between predicted and measured N_{CCN} produces a slope of 1.012 and an intercept of 128.3 cm^{-3} ($R^2=0.95$), and the average ratio of predicted versus measured N_{CCN} is 0.94 (Figure

10). The results indicate some moderate underestimate (about 6% on average) but the agreement is still excellent. The achieved closure calculation suggested that water soluble inorganic ions played a major role in contributing the κ value. In fact, 83.8% of the κ was expressed by $\text{SO}_4^{2-} + \text{NO}_3^- + \text{NH}_4^+$ in total (in another study by our group, not published yet), with their individual contribution to be 39.8%, 31.7% and 12.3%, respectively. In addition, it is worth note that the predicted N_{CCN} at SS 0.2% was more correlated with the observed N_{CCN} in the clear case ($R^2=0.96$) than the foggy-hazy/hazy cases ($R^2=0.91$), and the corresponding ratios of predicted to observed N_{CCN} were 0.95 and 0.92, respectively (Figure 11). In all cases, the mean ratio of predicted to observed N_{CCN} never reached up to 1, suggesting that organic matter would play a second role and make up the rest of κ .

4. Conclusions and discussion

A continuous 4-day data obtained at an urban site of Shanghai over a fog-haze event from 6 to 9 November 2012 was analyzed for CCN and aerosol. Overall, meteorological conditions such as wind speed, wind direction and temperature exerted a great influence on $\text{PM}_{2.5}$ and BC loadings. Human activity is an essential factor to control emissions of aerosol and CCN in urban environments. $N_{\text{CCN}}/N_{\text{CN}}$ and N_{CCN} usually were higher in the hazy case due to increased aerosols in the accumulation mode, and lower in the foggy-hazy and clear cases. Of

special interest, the low N_{CCN}/N_{CN} , N_{CN} and N_{CCN} during the foggy-hazy case can plausibly explain in three aspects: (1) the limited data input introduces some uncertainties, (2) the possible physical effects such as boundary layer evolution, transportation and atmospheric dilution (i.e. the effect of diurnal variations) are not considered, (3) the plausible emergence of fog droplets and particles leads to the reduction of aerosol number concentration.

BC was correlated well with N_{CCN} in the foggy-hazy and hazy cases but the clear case, as not N_{CCN}/N_{CN} did. More BC is aged during the foggy-hazy/hazy cases, hence more CCN is activated (Dusek et al., 2006; Anttila and Kerminen., 2007; Hudson., 2007). However, there exists a different perspective. For example, BC has been found to significantly suppress cloud formation in the Indo-Gangetic plain (Ritesh et al., 2007). Pure BC particles are hydrophobic and can release heat by absorbing solar radiation, hence they would increase the critical SS of aerosol to act as CCN and further suppress the tendency of CCN to become cloud droplets. However, aged BC particles are sufficiently hydrophilic by acquiring hydrophilic coatings in the atmosphere, and become CCN and favor aerosol indirect forcing (Conant et al., 2002; Ritesh et al., 2007). In this study, BC particles moved a long-distance from inland and aged during the transporting process, thereby it favors CCN formation.

By using a simplified κ parameter, the critical dry size never exceeded

130 nm. In spite of the absence of organic matter, the CCN closure calculation was still achieved, suggesting that aerosol major water soluble ions contribute to effective κ . The predicted N_{CCN} was close to the observed during the clear case than the foggy-hazy/hazy cases having more organic matter. In summary, water soluble inorganic ions constituted the majority of particle hygroscopicity (κ) estimation, while organic matter made up the rest. It is noted that organic matter is essential to build the exact CCN prediction models.

This paper mainly explored how N_{CCN} , N_{CN} and N_{CCN}/N_{CN} vary under a fog-haze co-occurring condition, as well as the major influential factors to these activities. The results revealed that the particulate pollutant burden exerts a significant impact on N_{CCN} , especially N_{CCN}/N_{CN} is effectively promoted during the polluted periods (e.g. haze). Importantly, the fog-haze transformation is highly complicated involving numerous changes of aerosol in physical and chemical properties, which remains poorly understood. There presents the results of only a case, so more efforts are needed for highlighting the comprehensive effects of fog and haze on CCN in urban environments.

Acknowledgements

This research is supported by the National Basic Research Program of China (2010CB428503), the National Natural Science Foundation of

China (41075096, 21190053, 21177025, 21277028, 21377029, [41475109](#)), and partly by the Research and Development Special Fund for Public Welfare Industry (Meteorology) of CMA (GYHY201006047), the Shanghai Science and Technology Commission of Shanghai Municipality (12DJ1400100, 12DZ2260200), the Jiangsu Collaborative Innovation Center for Climate Change, and Priority fields for Ph.D. Programs Foundation of Ministry of Education of China (0110071130003) and FP7 project (AMIS, PIRSES-GA-2011).

Reference

Andreae, M. O., et al.: Correlation between cloud condensation nuclei concentration and aerosol optical thickness in remote and polluted regions, *Atmos. Chem. Phys.*, 9, 543-556, doi: 10.5194/acp-9-543-2009, 2009.

Andreae, M. O., et al.: Smoking rain clouds over the Amazon, *Science.*, 303, 1337-1342, doi: 10.1126/science. 1092779, 2004.

Andreae, M. O., Jones, C. D., and Cox. P. M.: Strong present-day aerosol cooling implies a hot future, *Nature.*, 435, 1187-1190, 2005.

Anttila, T., and Kerminen, V. M.: On the contribution of Aitken mode particles to cloud droplet populations at continental back-ground areas-a parametric sensitivity study, *Atmos. Chem. Phys.*, 7, 4625-4637, 2007.

Baumgardner, D., Raga, G. B., and Muhlia, A.: Evidence for the

formation of CCN by photochemical processes in Mexico City, Atmos.
Environ., doi:10.1016, 2003.

Biswas, K. F., Ghauri, B. M., and Husain, L.: Gaseous and aerosol
pollutants during fog and clear episodes in South Asian urban
atmosphere, Atmos. Environ., 42, 7775-7785, 2008.

[Boers, R., and Eloranta, E.W.: Lidar measurements of the atmospheric
entrainment zone and the potential temperature jump across the top of
the mixed layer, Boundary-Layer Meteorology, 34, 357-375, 1986.](#)

[Brooks, I.M.: Finding boundary layer top: application of a wavelet
covariance transform to lidar backscatter profiles, Journal of
Atmospheric and Oceanic Technology, 20, 1092-1105, 2003.](#)

Burkar, J., Steiner, G., Reischl, G., and Hitzenberger, R.: Long-term study
of cloud condensation nuclei (CCN) activation of atmospheric aerosol in
Vienna, Atmos. Environ., 45, 5751-5759, 2011.

[Campbell, J.R., Hlavka, D.L., Welton, E.J., Flynn, C.J., Turner, D.D.,
Spinhirne, J.D., Scott, V.S., and Hwang, I.H.: Full-time, eye-safe cloud
and aerosol lidar observation at atmospheric radiation measurement
program sites: Instruments and data processing, J. Atmos. Oceanic
Technol., 19, 431-442, 2002.](#)

Che, H. Z., Zhang, X. Y., Li, Y., Zhou, Z. J., Qu, John. J and Hao, X. J.:
Haze trends over the capital cities of 31 provinces in China, 1981-2005,
Theor. Appl. Climatol., 97, 235-242, 2009.

639 Cheng, T. T., Han, Z. W., Zhang, R. J., Du, H. H., Jia, X., Wang, J. J., and
640 Yao, J. Y.: Black carbon in a continental semi-arid area of Northeast
641 China and its possible sources of fire emission, *J. Geophys. Res.*, 115,
642 D23204, doi: 10.1029/2009JD013523, 2010.

643 Cheng, Y., Lee, S. C., Ho, K. F., Wang, Y. Q., Cao, J. J., Chow, J. C., and
644 Watson, J. G.: Black carbon measurement in a coastal area of south
645 China, *J. Geophys. Res.*, 111, D12310, doi: 10.1029/2005JD006663,
646 2006.

647 Cohn, S.A., Angevine W.M.: Boundary layer height and entrainment zone
648 thickness measured by lidars and wind-profiling radars. *Journal of*
649 *Applied Meteorology*, 39, 1233-1247, 2000.

650 Conant, W. C., A. Netes, and J. H. Seinfeld.: Black carbon radiative
651 heating effectson cloud microphysics and implications for the aerosol
652 indirect effect: 1. Extented Köhler theory, *J. Geophys. Res.*, 107 (D21),
653 4604, doi:10.1029/2002JD002094, 2002.

654 Cubison, M. J., Ervens, B., Feingold, G., Docherty, K .S., Ulbrich, I. M.,
655 Shields, L., Prather, K., Hering, S. and Jimenez, J. L.: The influence of
656 chemical composition and mixing state of Los Angeles urban aerosol on
657 CCN number and cloud properties, *Atmos. Chem. Phys.*, 8, 5649-5667,
658 2008.

659 Deng, Z. Z., Zhao, C. S., Ma, N.P., Liu, F., Ran, L., Xu, W. Y., Liang, Z.,
660 Liang, S., Huang, M. Y., Ma, X.C., Zhang, Q., Quan, J. N., and Yan, P.:

661 Size- resolved and bulk activation properties of aerosols in the North
662 China Plain, *Atmos. Chem. Phys.*, 11, 3835-3846, 2011.

663 Draxler, R. R., and Rolph, G. D.: HYSPLIT(Hybrid Single-Particle
664 Lagrangian Integrated Trajectory) Model access via NOAA ARL
665 READY Website (<http://www.arl.noaa.gov/ready/hysplit4.htm>), NOAA
666 Air Resources Laboratory, Silver Spring, MD, 2003.

667 Du, H., Kong, L., Cheng, T., Chen, J., Du, J., et al.: Insights into
668 summertime haze pollution events over Shanghai based on online
669 water-soluble ionic composition of aerosols, *Atmos. Environ.*, 45,
670 5131-5137, 2011.

671 Dumka, U.C., Krishna Moorthy, K., Rajesh Kumar, Hegde, P., Ram Sagar,
672 Pant, P., et al.: Characteristics of aerosol black carbon mass
673 concentration over a high altitude location in the Central Himalayas
674 from multi-year measurements, *Atmos. Res.*, 96, 510-521, 2010.

675 Dusek, U., Frank, G. P., and Hildebrandt, L.: Size matters more than
676 chemistry for cloud- nucleating ability of aerosol particles, *Science*, 312,
677 1375-1378, 2006.

678 Elizabeth, R. G., Paula, K. H., and Vicki, H. G.: Physicochemical
679 properties of nitrate aerosols: Implications for the atmosphere, *J. Phys.*
680 *Chem.*, 110, 11785-11799, 2006.

681 Ferin, J., Oberdoerster, G., Penney, D. P., Soderholm, S. C., Gelein, R.,
682 and Piper, H. C.: Increased pulmonary toxicity of ultrafine particles 1.

683 Particles clearance, translocation, morphology, *J. Aerosol Sci.*, 21 (3),
684 381-384, 1990.

685 Fernald, F. G.: Analysis of atmospheric lidar observations: Some
686 comments, *Appl. Opt.*, 23(5), 652-653, 1984.

687 Fisak, J., Tesar, M., Rezacova, D., Elias, V., Weignerova, V., and Fottova,
688 D.: Pollutant concentrations in fog and low cloud water at selected sites
689 of the Czech Republic, *Atmos. Res.*, 64, 75-87, 2002.

690 Fu, Q. Y., Zhuang, G. S., Wang, J., Xu, C., Huang, K., Li, J., Hou, B., Lu,
691 T., and Streets, D. G.: Mechanism of formation of the heaviest
692 pollution episode ever recorded in the Yangtze River Delta, China,
693 *Atmos. Environ.*, 42, 2023-2036, 2008.

694 Furutani. H., Dall'Osto, M., Roberts, G. C., and Prather, K. A.:
695 Assessment of the relative importance of atmospheric aging on CCN
696 activity derived from field observations, *Atmos. Environ.*, 42,
697 3130-3142, 2008.

698 Gao, J., Wang, T., Zhou, X. H., Wu, W. S., and Wang, W. X.:
699 Measurement of aerosol number size distributions in the Yangtze River
700 delta in China: formation and growth of particles under polluted
701 conditions, *Atmos. Environ.*, 43 (4), 829-836, 2009.

702 Gautam, R., Hsu, N. C., Kafatos, M. and Tsay, S. C.: Influences of winter
703 haze on fog/low cloud over the Indo-Gangetic plains, *J. Geophys. Res.*,
704 112, D05207, doi: 10.1029/2005JD007036, 2007.

Gulpete, I., Tardif, R., Michaelides, S. C., Cermak, J., Bott, A., Bendix, J.,
Müller, M. D., Pagowski, M., Hansen, B., Ellrod, G., Jacobs, W., Toth,
G., and Cober, S. G.: Fog research: a review of past achievements and
future perspectives, *Pure and Applied Geophys.*, 164, 1121-1159, 2007.

Hagler, G. S. W., Bergin, M. H., Smith, E. A. and Dibb, J. E.: A summer
time series of particulate carbon in the air and snow at Summit,
Greenland, *J. Geophys. Res.*, 112, D21309, doi: 10.1029/2007JD008993,
2007.

Hansen, A. D. A., Rosen, H., and Novakov T.: The aethalometer-an
instrument for the real-time measurement of optical absorption by
aerosol particles, *Sci. Total Environ.*, 36, 191-196, 1984.

He, Q. S., Li, C. C., Mao, J. T., Lau, A. K. H., and Li, P. R.: A study on
the aerosol extinction-to-backscatter ratio with combination of
micro-pulse LIDAR and MODIS over Hong Kong, *Atmos. Chem. Phys.*,
6, 3243-3256, 2006.

Henning, S., Wex, H., Hennig, T., Kiselev, A., Snider, J. R., Rose, D., et
al.: Soluble mass, hygroscopic growth, and droplet activation of coated
soot particles during LACIS Experiment in November (LExNo), *J.*
Geophys. Res., 115, D11206, doi: 10.1029/2009JD012626, 2010.

Herckes, P., Chang, H., Lee, T., and Collett Jr., J. L.: Air pollution
processing by radiation fogs, *Water, Air, & Soil Pollution* 181 (1), 65-75,
2007.

727 Hings, S. S., Wrobel, W. C., Cross, E. S., Worsnop, D. R., Davidovits, P.
728 and Onasch, T. B.: CCN activation experiments with adipic acid: effect
729 of particle phase and adipic acid coatings on soluble and insoluble
730 particles, *Atmos. Chem. Phys.*, 8, 3735-3748, 2008.

731 Hitzenberger, R., Giebl, H., Petzold, A., Gysel, M., Nyeki, S.,
732 Weingartner, E., Baltensperger, U., and Wilson, W. C.: Properties of jet
733 engine combustor particles during the PartEmis experiment.
734 Hygroscopic properties at supersaturated conditions, *Geophys. Res.*
735 *Lett.*, 30 (14), 1779, doi: 10.1029/2003GL017294, 2003.

736 Hudson, J.: Variability of the relationship between particle size and
737 cloud-nucleating ability, *Geophys. Res. Lett.*, 34, L08801, doi:
738 10.1029/2006GL028850, 2007.

739 [Hudson, J. G. and Noble, S.: CCN and vertical velocity influence on](#)
740 [droplet concentration and supersaturations in clean and polluted stratus](#)
741 [clouds, *J. Atmos. Sci.*, 106, 24119-24126, 2014.](#)

742 IPCC.: Climate Change 2007: The Physical Science Basis. In: Solomon,
743 S., et al., (Eds.). Contribution of Working Group I to the Fourth
744 Assessment Report of the Intergovernmental Panel on Climate Change,
745 Cambridge Univ. Press, Cambridge and New York, 2007.

746 Jimenez, J. L. et al.: Evolution of organic aerosols in the atmosphere,
747 *Science*, 326, 1525-1529, 2009.

748 Juranyi, Z., Gysel, M., Weingartner, E., DeCarlo, P. F., Kammermann, L.,

and Balternsperger, U.: Measurement and modeled cloud condensation nuclei concentration at the high alpine site Jungfraujoch, *Atmos. Chem. Phys. Discussions.*, 10, 8859-8897, 2010.

Köhler, H.: The nucleus in and the the growth of hygroscopic droplets, *T. Faraday Soc.*, 32, 1152-1161, 1936.

Kuang, C., McMurry, P. H., and McCormick, A.V.: Determination of cloud condensation nuclei production from measured new particle formation events, *Geophys. Res. Lett.*, 36, L09822, doi: 10.1029/2009GL037584, 2009.

Kuwata, M. and Kondo, Y.: Dependence of size-resolved CCN spectra on the mixing state of nonvolatile cores observed in Tokyo. *J. Geophys. Res.*, 113, D19202, doi: 10.1029/2007JD009761, 2008.

Kuwata, M., Kondo, Y., Mochida, M., Takegawa, N. and Kawamura, K.: Dependence of CCN activity of less volatile particles on the amount of coating observed in Tokyo, *J. Geophys. Res.*, 112, D11207, doi: 10.1029/2006JD007758, 2007.

Lance, S., Medina, J., Smith, J. N., and Nenes, A.: Mapping the operation of the DMT Continuous Flow CCN counter, *Aerosol Sci. Tech.*, 40, 242-254, 2006.

Lathem, T. L., and Nenes A.: Water vapor depletion in the DMT Continuous Flow CCN Chamber: Effects on supersaturation and droplet growth, *Aerosol Sci. Tech.*, 45(5), 604-615, 2011.

771 Leng, C. P., Cheng, T. T., Chen, J. M., et al.: Measurements of surface
772 cloud condensation nuclei and aerosol activity in downtown Shanghai,
773 Atmos. Environ., 69, 354-361, 2013.

774 Liu, J. J., Zheng, Y. F., Li, Z. Q., and Cribb, M.: Analysis of cloud
775 condensation nuclei properties at a polluted site in southeastern China
776 during the AMF-China Campaign, J. Geophys. Res., 116, D00K35, doi:
777 10.1029/2011JD016395, 2011.

778 Lohmann, U. and Feichter, J.: Global indirect aerosol effect; a review,
779 Atmos. Chem. Phys., 5, 715-737, 2005.

780 Matsui, H., Koike, M., Kondo, Y., Takegawa, N., Fast, J. D., Pöschl, U.,
781 Garland, R. M., Andreae, M. O., Wiedensohler, A., Sugimoto, N., and
782 Zhu, T.: Spatial and temporal variations of aerosols around Beijing in
783 summer 2006: 2. Local and column aerosol optical properties, J.
784 Geophys. Res., 115, D22207, doi: 10.1029/2010JD013895, 2010.

785 Menut, L., Flamant, C., Pelon, J., Flamant, P. H.: Urban boundary-layer
786 height determination from lidar measurements over the Paris area. Appl.
787 Optics. 38, 945-954, 1999.

788 Merikanto, J., Sprackken, D. V., Mann, G. W., Pickering, S. J and Carslaw,
789 K. S.: Impact of nucleation on global CCN, Atmos. Chem. Phys., 9(21),
790 8601-8616, 2009.

791 Moffet, R. C., de Foy, B., Molina, L. T., Molina, M. J. and Prather, A.:
792 Measurements of ambient aerosols in northern Mexico City by single

793 particle mass spectrometry, *Atmos. Chem. Phys.*, 8, 4499-4516, 2008.

794 Petters, M. D., and S. M. Kreidenweis.: A single parameter representation
795 of hygroscopic growth and cloud condensation nucleus activity, *Atmos.*
796 *Chem. Phys.*, 7, 1961-1971, 2007.

797 Petzold, A., Kopp, C. and Niessner R.: The dependence of the specific
798 attenuation cross-section on black carbon mass fraction and particle
799 size, *Atmos. Environ.*, 31(5), 661-672, 1997.

800 Pierce, J. R., et al.: Contribution of primary carbonaceous aerosol to
801 cloud condensation nuclei: Processes and uncertainties evaluated with
802 a global aerosol microphysics model, *Atmos.Chem. Phys.*, 7,
803 5447-5466, doi: 10.5194/acp-7-5447-2007, 2007.

804 Qian, Y., Kaiser, D. P., Leung, L. R., and Xu, M.: More frequent
805 cloud-free sky and less surface solar radiation in China from 1955-2000,
806 *Geophys. Res. Lett.*, 33, L01812, doi:10.1029/2005GL024586, 2006.

807 Quinn, P. K., Bates, T. S., Coffman, D. J. and Covert, D. S.: Influence of
808 particle size and chemistry on the cloud nucleating properties of aerosols,
809 *Atmos. Chem. Phys.*, 8, 1029-1042, 2008.

810 Reade, L., Jennings, S. G., and Gobnait, M.: Cloud condensation nuclei
811 measurements at Mace Head, Ireland, over the period 1994-2002, *Atmos.*
812 *Res.*, 82, 610-621, 2006.

813 Ritesh, G., Christina, H., Menas. Kafatos., Si-Chee. T.: Influences of
814 winter haze on fog/low cloud over the Indo-Gangetic plains. *J. Geophys.*

815 Res., 112, D05207, doi: 10. 1029/2005JD007036, 2007.

816 Roberts, G. C. and Nenes, A.: A continuous-flow streamwise
817 thermal-gradient CCN chamber for atmospheric measurements, *Aerosol*
818 *Sci. Tech.*, 39, 206-221, 2005.

819 Rose, D., Gunthe, S. S., Su. H., Carland. R. M., Yang. H., et al.: Cloud
820 condensation nuclei in polluted air and biomass burning smoke near the
821 mega-city Guangzhou, China- Part 2: Size-resolved aerosol chemical
822 composition, diurnal cycles, and externally mixed weakly CCN-active
823 soot particles, *Atmos. Chem. Phys.*, 11, 2817-2836, 2011.

824 Rose, D., Nowak, A., Achtert. P., Wiedensohler. A., Hu. M., et al.: Cloud
825 condensation nuclei in polluted air and biomass burning smoke near the
826 mega-city Guangzhou, China- Part 1: Size-resolved measurements and
827 implications for the modeling of aerosol particle hygroscopicity and
828 CCN activity, *Atmos. Chem. Phys.*, 10, 3365-3383, 2010.

829 Rosenfeld, D., Dai, J., Yu, X., Yao, Z., Xu, X., Wang, X., and Du, C.:
830 Inverse relations between amounts of air pollution and orographic
831 precipitation, *Science*, 315, 1396-1398, 2007.

832 Rosenfeld, D., Lohmann, U., Raga, G. B., O'Dowd, C. D., Kulmala, M.,
833 Fuzzi, S., Reissell, A., and Andreae, M. O.: Flood or Drought: How Do
834 Aerosol Affects Precipitation?, *Science*, 321, 5894, 2008.

835 Shao, M., Tang, X., Zhang, Y., and Li, W.: City clusters in China: air and
836 surface water pollution, *Front. Ecol. Environ*, 4, 353-361, 2006.

837 Sihto, S. L., Mikkilä, J., Vanhanen, J., et al.: Seasonal variation of CCN
838 concentrations and aerosols activation properties in boreal forest, *Atmos.*
839 *Chem. Phys.*, 11, 13269-13285, 2011.

840 Stone, E. A., Snyder, D. C., Sheesley, R. J., Sullivan, A. P., Weber, R. J.
841 and Schauer, J. J.: Source apportionment of fine organic aerosol in
842 Mexico City during the MILAGRO experiment 2006, *Atmos. Chem.*
843 *Phys.*, 8, 1249-1259, 2008.

844 Streets, D. G., Tsia, N. Y., Akimoto, H., and Oka, K.: Sulfur dioxide
845 emissions in Asia in the period 1985-1997, *Atmos. Environ.*, 34,
846 4413-4424, 2000.

847 Streets, D. G., Yu, C., Wu, Y., Chin, M., Zhao, Z., Hayasaka, T., and Shi,
848 G.: Aerosol trends over China, 1980-2000, *Atmos. Res.*, 88, 174-182,
849 2008.

850 Sun, Y. L., Zhuang, G. S., Tang, A. H., Wang, Y., and An, Z. S.: Chemical
851 characteristics of PM_{2.5} in haze-fog episodes in Beijing, *Environ. Sci.*
852 *Tech.*, 40, 3148-3155, 2006.

853 Svenningsson, B., Rissler, J., Swietlicki, E., Mircea, M., Bilde, M., et al.:
854 Hygroscopic growth and critical supersaturations for mixed aerosol
855 particles of inorganic and organic compounds of atmospheric relevance,
856 *Atmos. Chem. Phys.*, 6, 1937-1952, 2006.

857 Tie, X. and Cao, J.: Aerosol pollution in China: present and future impact
858 on environment, *Particuology*, 7, 426-43, 2009.

859 Urone, P., Lutsep, Helmut., Noyes. C. M., and Parcher, J. F.: Static
860 studies of sulfur dioxide reactions in air, *Environ. Sci. Tech*, 2(8),
861 611-618, 1968.

862 Wang, Y., Zhuang, G. S., Zhang, X. Y., Huang, K., Xu, C., Tang, A. H.,
863 Chen, J. M., and An, Z. S.: The ion chemistry, seasonal cycle, and
864 sources of PM_{2.5} TSP aerosol in Shanghai, *Atmos. Enviro.*,40,
865 2935-2952, 2006.

866 Weingartner, E., Saathoff, H., Schnaiter, M., Streit, N., Bitnar, B., and
867 Baltensperger U.: Absorption of light by soot particles: determination of
868 the absorption coefficient by means of aethalometers, *J. Aerosol Sci.*, 34,
869 1445-1463, 2003.

870 Wiedensohler, A., Cheng, Y. F., Nowak, A., Wehner. B., Achtert, P.,
871 Berghof, M., Birmili, W., Wu, Z. J., et al.: Rapid aerosol growth and
872 increase of cloud condensation nucleus activity by secondary aerosol
873 formation and condensation: A case study for regional air pollution in
874 northeastern China, *Geophys. Res. Lett.*,114, D00G08, doi:
875 10.1029/2008JD010884, 2009.

876 Ye, X. N., Ma, Z., Zhang, J. C., Du, H. H., Chen, J. M., Chen, H., Yang,
877 X., Gao, W., and Geng, F. H.: Important role of ammonia on haze
878 formation in Shanghai, *Environ. Lett.*, 6, 024019, 2011.

879 Yu, F. Q., Wang, Z., Luo, G., and Turco, R.: Ion-mediated nucleation as
880 an important global source of tropospheric aerosols, *Atmos. Chem.*

881 Phys., 8, 2537-2554, 2008.

882 Yue. D. L., Hu. M., Zhang. R. J., Wu. Z. J., Su. H., et al.: Potential
883 contribution of new particle formation to cloud condensation nuclei in
884 Beijing, Atmos. Environ., 45, 6070-6077, 2011.

885 Yum. S. S., James, G. H., Keun, Y. S., and Byoung-Cheol, C.:
886 Springtime cloud condensation nuclei concentrations on the west coast
887 of Korea, Geophys. Res. Lett., 32, L09814, doi: 10.
888 1029/2005GL022641, 2005.

889 Yum. S. S., and James, G. H.: Wintertime/summertime contrasts of cloud
890 condensation nuclei and cloud microphysics over the South Ocean, J.
891 Geophys. Res., 109, D06204, doi: 10.1029/2003JD003864, 2004.

892 Zhang, M., Wang, X., Chen, J., Cheng, T., Wang, T. et al.: Physical
893 characterization of aerosol particles during the Chinese New Year's
894 firework events, Atmos. Environ., 44, 5191-5198, 2010a.

895 Zhang, Q., Tie, X. X., Lin, W. L., Cao, J. J., Quan, J. N., Ran, L., and Xu,
896 W. Y.: Variability of SO₂ in an intensive fog in North China Plain:
897 Evidence of high solubility of SO₂, Particuology, 11, 41-47, 2013.

898 Zhang, R. J., Jing, J. S., Tao, J., Hsu, S.-C., Wang, G., Cao, J. J., Lee, C. S.
899 L., et al.: Chemical characterization and source apportionment of PM_{2.5}
900 in Beijing: seasonal perspective, Atmos. Chem. Phys., 13, 7053-7074,
901 2013.

902 Zhang, X. Y., Zhuang G. S., Chen, J. M., Wang, Y. X., An, Z. S., Zhang, P.:

Heterogeneous reactions of sulfur dioxide on typical mineral particles, J. Phys. Chem., B, 110, 12588-12596, 2006b.

Table 1 Statistics of meteorological parameters in different weather conditions.

	Clear day	Foggy-hazy day	Hazy day	All
Temperature (°C)	14.39	14.59	16.53	15.02
Wind direction (deg)	157.22	191.36	260.59	191.27
Wind speed (m/s)	1.95	1.28	2.27	1.94
Pressure (hPa)	1021.92	1019.19	1019.45	1020.83
RH (%)	58.13	84.93	58.33	61.95
Visibility (km)	15.41	2.33	4.44	10.42
PBL (km)	1.2	0.58	0.62	0.93
Extinction coefficient	0.32	0.27	0.76	0.62

Table 2 Statistics of CCN, CN, CCN/CN and BC in different weather conditions.

	Clear day	Foggy-hazy day	Hazy day	All
CCN range (cm ⁻³)	994-5096	1677-2947	2088-6268	994-6268
CCN average (cm ⁻³)	2432	2377	4362	2929
CN range (cm ⁻³)	4270-15,168	4815-13,922	6033-15,771	4270-15,771
CN average (cm ⁻³)	8956	8367	10500	9344
CCN/CN range	0.09-0.48	0.18-0.40	0.25-0.57	0.09-0.57
CCN/CN average	0.28	0.29	0.41	0.32
BC range (μg/m ⁻³)	4.51-20.40	6.7-14.7	8.3-35.2	4.51-35.20
BC average (μg/m ⁻³)	8.57	9.58	21.26	12.24

Table 3 Effective hygroscopicity parameters (κ_i), and densities of the three category compositions in fine particles (Yue et al., 2011)

Species	Data source	κ_i	Density (g cm ⁻³)
Sulfate & Nitrate	SO ₄ ²⁻ +NO ₃ ⁻ +NH ₄ ⁺	0.6	1.7
Sodium chloride and marine aerosols	Na ⁺ +Cl ⁻	1.0	2.2

Insoluble compounds	BC	0	1.0
	others	0	2.0

Figure captions

Figure 1 Agricultural fire scattering areas and air mass transport pathways across these regions. All red spots represent biomass burning sites on 7 November measured from MODIS satellite. Starting time (LT) is labeled in the figure.

Figure 2 Temporal variations of temperature, wind speed and direction, RH, pressure and atmospheric visibility.

Figure 3 Temporal variations of PBL and vertical extinction coefficient measured by MPL lidar.

Figure 4 Hourly mean particle number concentrations of different sub-size bins.

Figure 5 Average size distributions for all the hazy, foggy-hazy, and clear cases.

Figure 6 Temporal variations of particle water soluble ion composition and trace gases.

Figure 7 Temporal variations of N_{CN} , N_{CCN} at 0.2% SS, BC, $PM_{2.5}$ and N_{CCN}/N_{CN} .

Figure 8 Temporal variations of $CN_{100nm-10\mu m}$, $CN_{80nm-10\mu m}$, $CCN/CN_{100nm-10\mu m}$ at 0.2% SS and $CCN/CN_{80nm-10\mu m}$ at 0.2% SS.

Figure 9 Correlations of BC mass concentration (M_{BC}) to N_{CCN} and N_{CCN}/N_{CN} (0.2% SS).

Figure 10 Scatterplot of the simplified closure analysis at SS 0.2%.

Figure 11 Correlations of observed and predicted N_{CCN} (0.2% SS) in the clear (a) and foggy-hazy/hazy (b) cases.

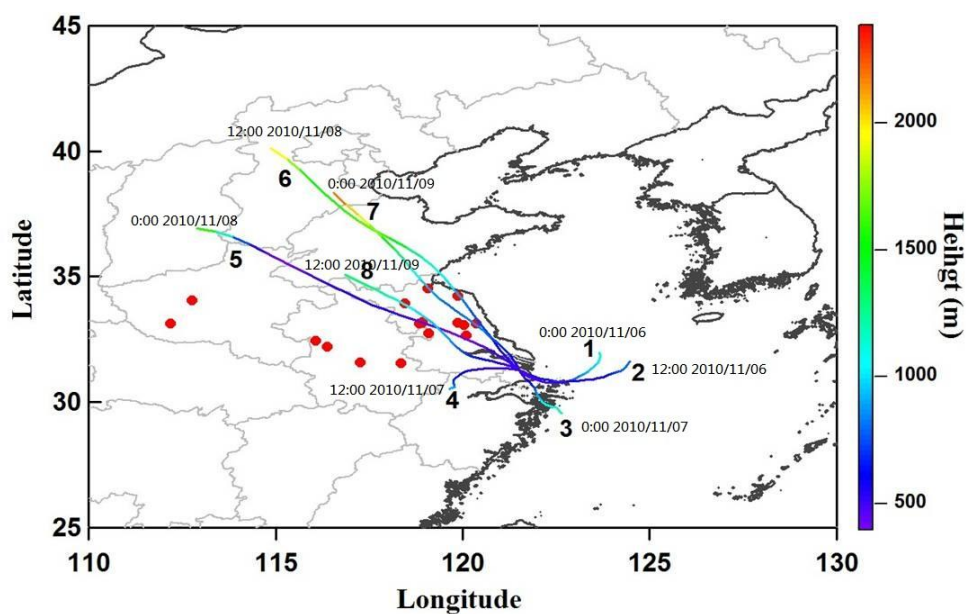


Figure 1 Agricultural fire scattering areas and air mass transport pathways across these regions. All red spots represent biomass burning sites on 7 November measured from MODIS satellite. Starting time (LT) is labeled in the figure.

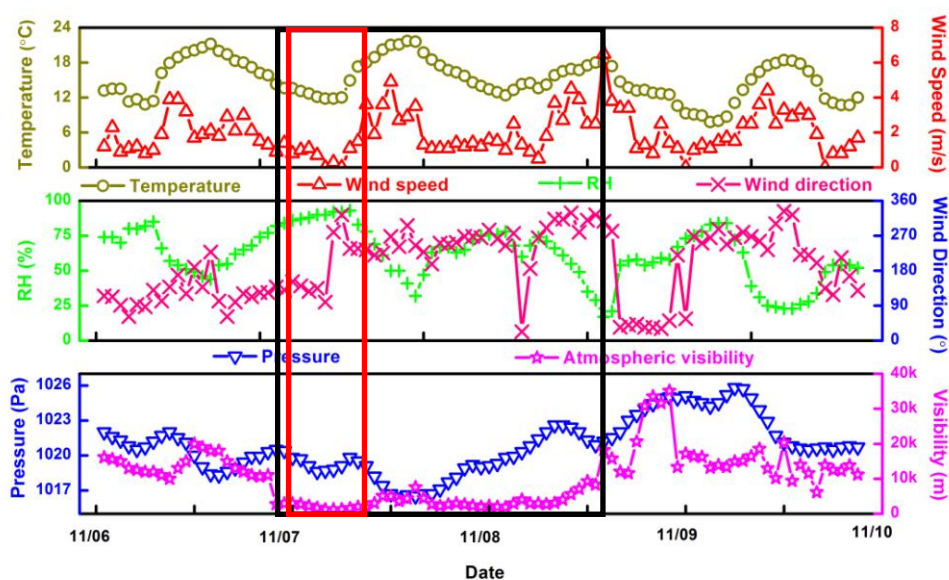


Figure 2 Temporal variations of temperature, wind speed and direction, RH, pressure and atmospheric visibility.

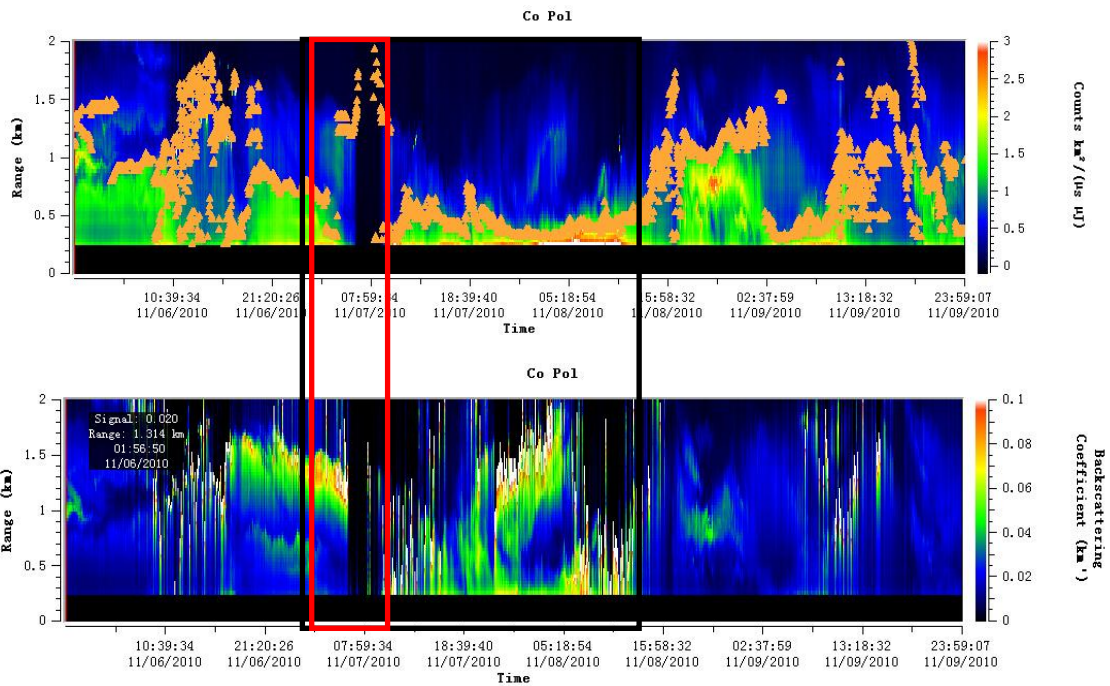


Figure 3 Temporal variations of PBL and vertical extinction coefficient measured by MPL lidar.

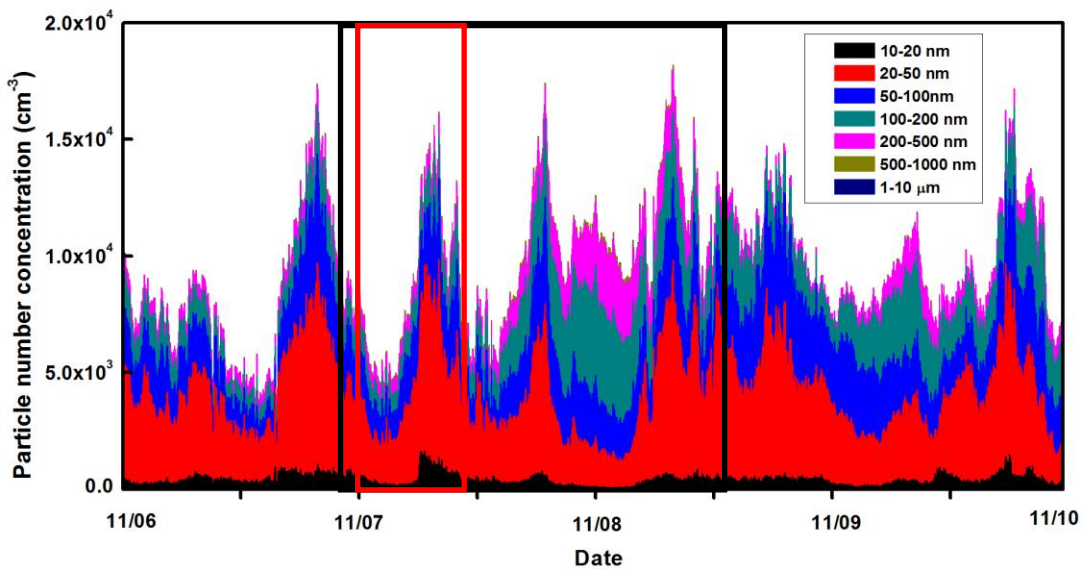


Figure 4 Hourly mean particle number concentrations of different sub-size bins.

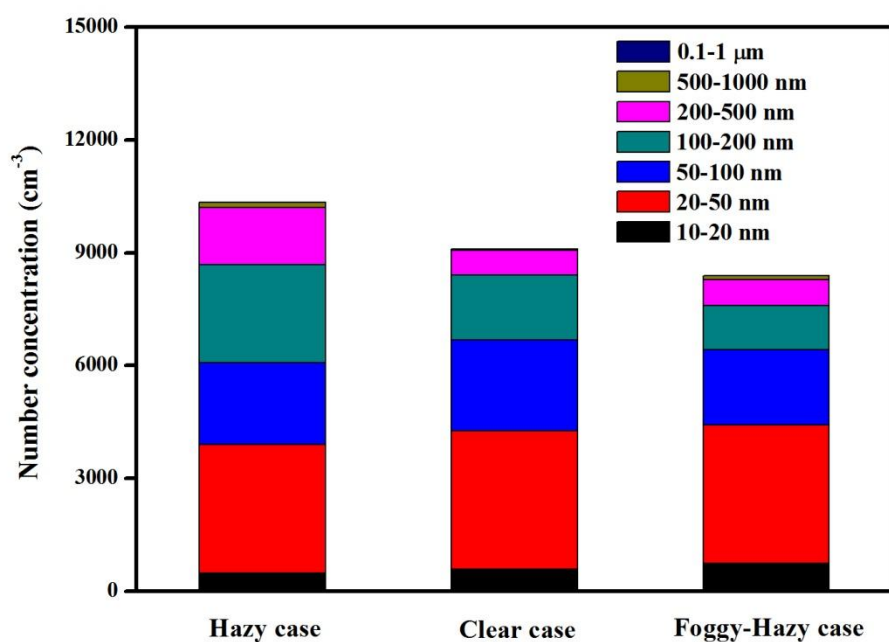


Figure 5 Average size distributions for all the hazy, foggy-hazy, and clear cases.

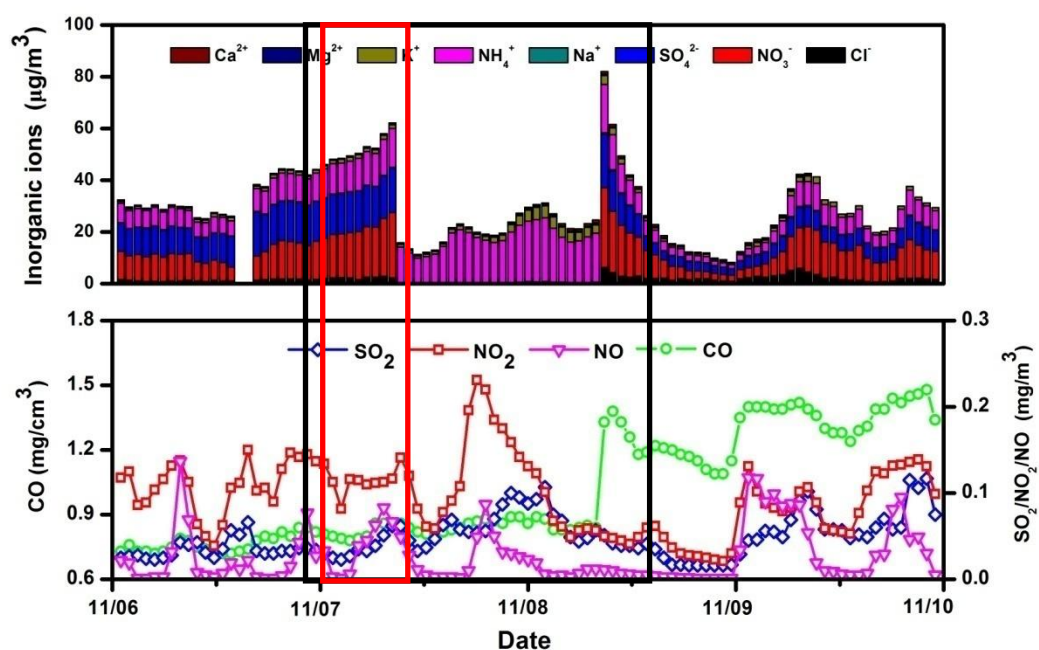


Figure 6 Temporal variations of particle water soluble ion composition and trace gases.

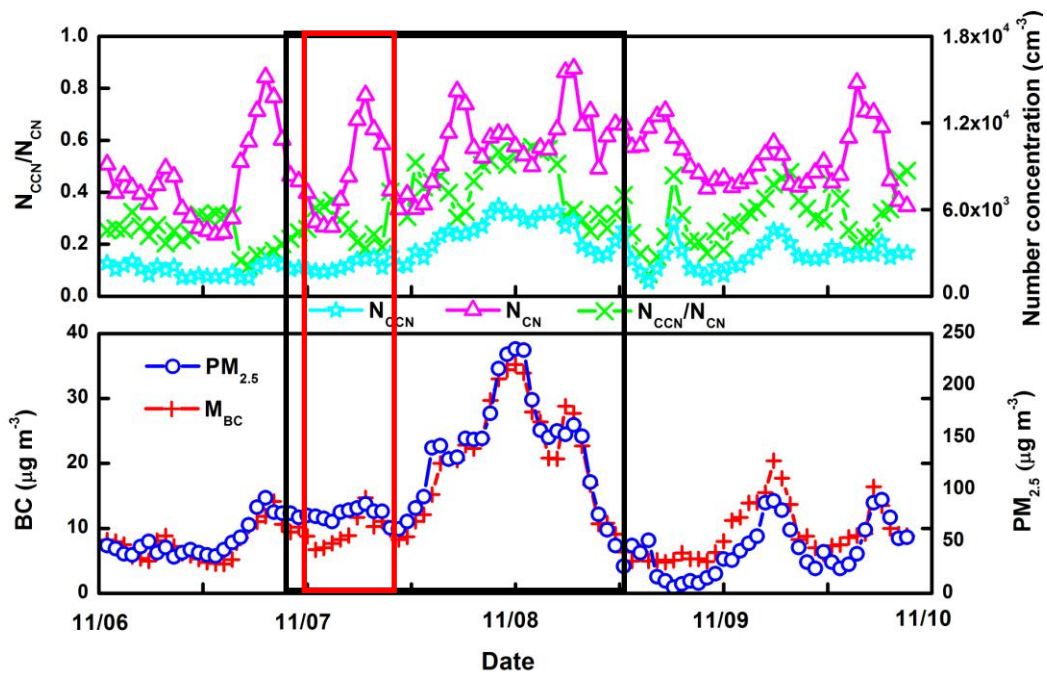


Figure 7 Temporal variations of N_{CN} , N_{CCN} at 0.2% SS, BC, $PM_{2.5}$ and N_{CCN}/N_{CN} .

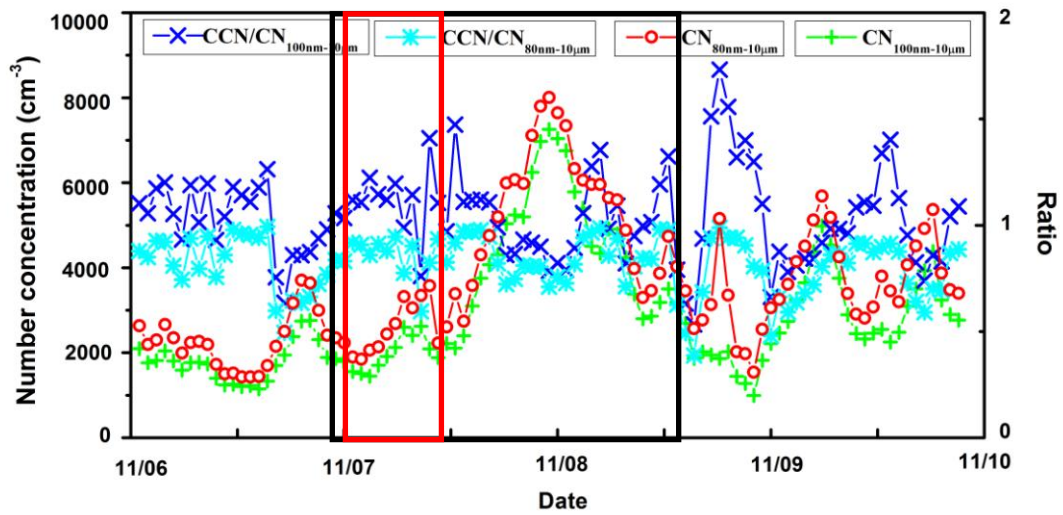


Figure 8 Temporal variations of $CN_{100nm-10\mu m}$, $CN_{80nm-10\mu m}$, $CCN/CN_{100nm-10\mu m}$ at 0.2% SS and $CCN/CN_{80nm-10\mu m}$ at 0.2% SS.

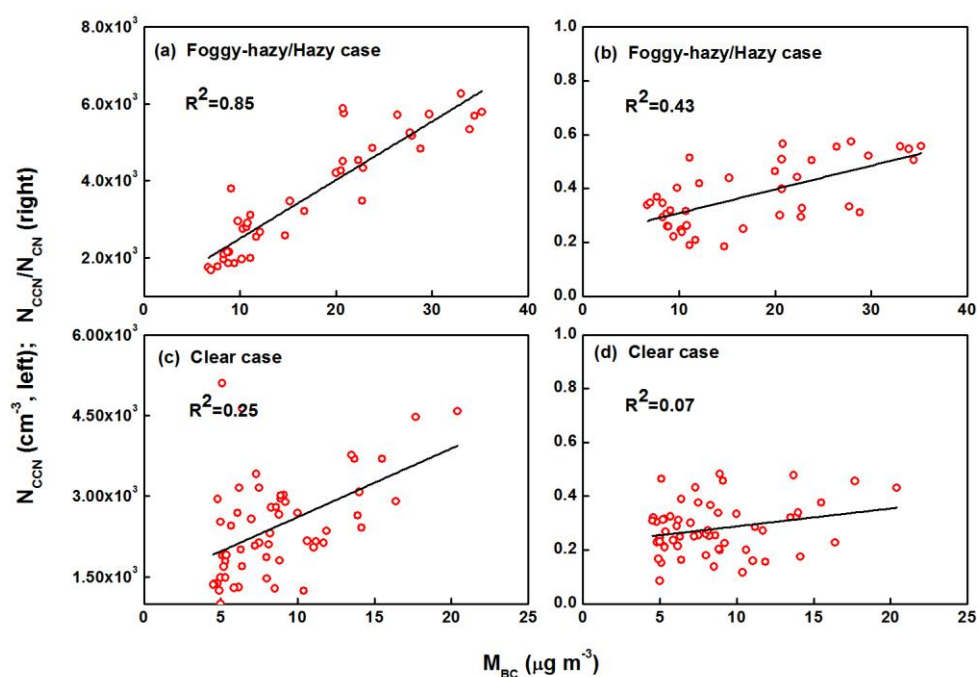


Figure 9 Correlations of BC mass concentration (M_{BC}) to N_{CCN} and N_{CCN}/N_{CN} (0.2% SS).

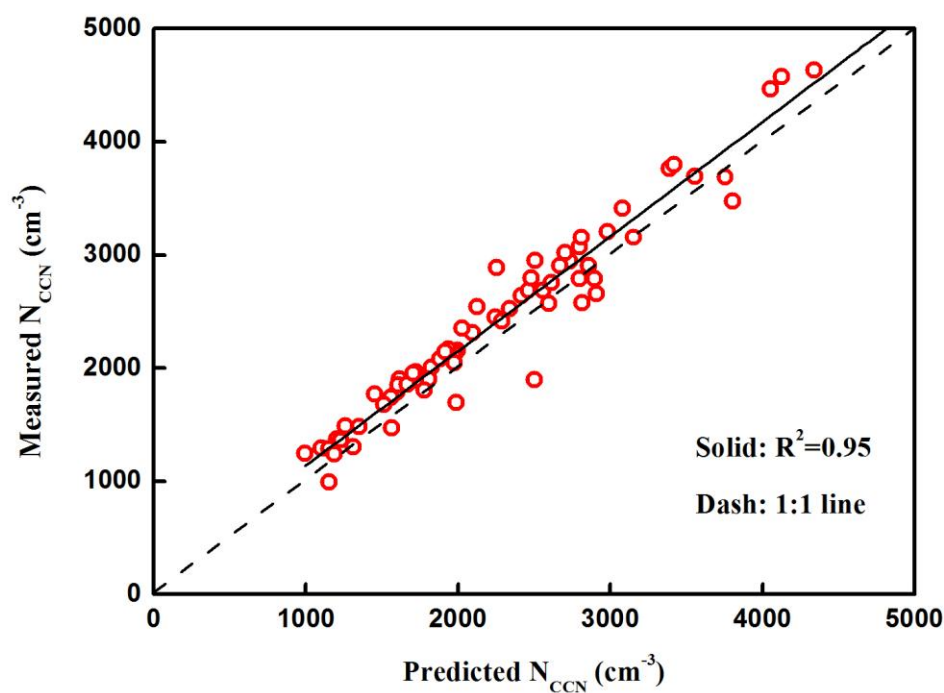
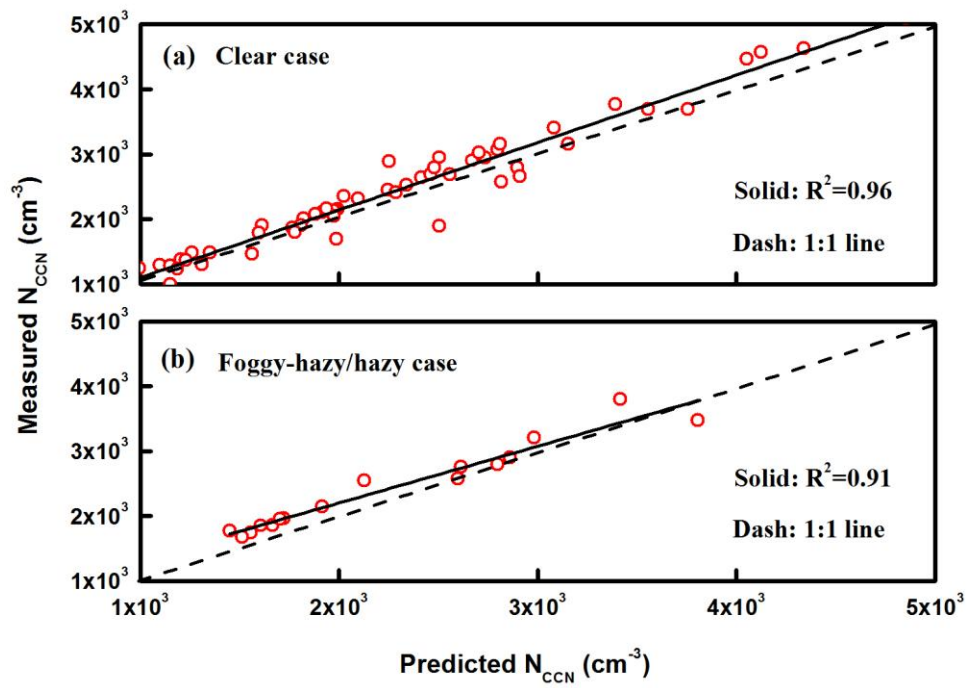


Figure 10 Scatterplot of the simplified closure analysis at SS 0.2%.

1019



1020

1021 **Figure 11** Correlations of observed and predicted N_{CCN} (0.2% SS) in the
 1022 clear (a) and foggy-hazy/hazy (b) cases.

1023

1024